of these detailed reactions. Improved acetylene concentrations lead to better soot production estimation. More chemical reactions, up to PAH formation, should be included for high hydrocarbon fuel chemical kinetics, especially for strong sooting cases, even though it makes the calculation more complicated and time consuming.

Figure 3 shows the soot volume fraction f_v and number density N_s for Held's kinetics and University of Utah kinetics, with the three treatments of radiation. For the present flame, the soot particles are produced on the fuel side of the flame sheet, between the stagnation plane and the flame sheet, and transported toward the stagnation plane away from the flame. As the stagnation plane is approached, soot particle size increases by coagulation and surface growth of soot particles. The soot particles are transported across the stagnation plane toward the fuel side by thermophoresis. At the current conditions, the coagulation rate of soot number density is much lower on the fuel side of the main soot formation region. This leads to higher soot number density, even near the stagnation plane. The University of Utah heptane kinetics predicts lower soot density compared to Held's kinetics. The peak soot volume fraction is 11% lower for the adiabatic/emission case, due to the lower acetylene species concentration. Radiation affects the soot volume fraction, even for this low soot density case. By the use of the University of Utah heptane kinetics, the emission-only calculation yields a peak soot volume fraction that is 10% lower than that based on the adiabatic calculation. The effects of absorption lead to a 5.9% higher peak soot volume fraction for the emission/absorption case compared to the emission-only calculations.

Summary

The calculations by the use of both Held's and University of Utah kinetics show good agreement for heptane flames. However, the detail chemical mechanism for the high hydrocarbon radicals is important to accurately predict the high hydrocarbon species and then the soot formation. The detail chemical reactions including PAH formation are necessary for high hydrocarbon fuel chemical kinetics, especially for high sooting combustion. The radiation heat loss including emission and absorption from soot particles strongly affects the soot formation.

Acknowledgments

This work was supported by the U.S. Department of Energy (DOE) Direct Injection Engine Research Program at Sandia National Laboratory under Grant DE FG04 99AL66266, with B. Carling and J. Keller serving as DOE Scientific Officers. The authors fully acknowledge the contributions of T. J. Held and A. F. Sarofim, who provided the n-heptane mechanisms and advice regarding their use.

References

[1]Davis, S. G., and Law, C. K., "Laminar Flame Speeds and Oxidation Kinetics of iso-Octane–Air and n-Heptane–Air Flames," *Proceedings of the Combustion Institute*, Vol. 27, 1998, pp. 521–527.

[2]Seiser, R., Truett, L., Trees, D., and Seshadri, K., "Structure and Extinction and Non-Premixed n-Heptane Flames," *Proceedings of the Combustion Institute*, Vol. 27, 1998, pp. 649–657.

[3]Li, S. C., and Williams, F. A., "Counterflow Heptane Flame Structure," *Proceedings of the Combustion Institute*, Vol. 28, 2000, pp. 1031–1038.

[4]Held, T. J., Marchese, A. J., and Dryer, F. L., "A Semi-Empirical Reaction Mechanism for n-Heptane Oxidation and Pyrolysis," *Combustion Science and Technology*, Vol. 123, 1997, pp. 107–146.

[5]Chevalier, C., Pitz, W. J., Warnatz, J., Westbrook, C. K., and Melenk, H., "Hydrocarbon Ignition: Automatic Generation of Reaction Mechanisms and Applications to Modeling of Engine Knock," *Proceedings of the Combustion Institute*, Vol. 24, 1992, pp. 93–101.

[6]Bakali, A. E., Delfau, J., and Vovelle, C., "Kinetics Modelings of a Rich, Atmospheric Pressure, Premixed n-Heptane/O_2/N_2 Flame," *Combustion and Flame*, Vol. 118, 1999, pp. 381–398.

[7]Baek, S. W., Park, J. H., and Choi, C. E., "Investigation of Droplet Combustion with Nongray Gas Radiation Effects," *Combustion Science and Technology*, Vol. 142, 1999, pp. 55–79.

[8]Belardini, P., Dertoli, C., Beatrice, C., D'anna, A., and Giacomo, N. D., "Application of a Reduced Kinetic Model for Soot Formation and Burnout in Three-Dimensional Diesel Combustion Computations," *Proceedings of the Combustion Institute*, Vol. 26, 1996, pp. 2517–2524.

[9]Zhu, X. L., Kim, O. J., Frankel, S. H., Viskanta, R., and Gore, J. P., "Radiation Effects on Combustion and Pollutant Emissions," *Second Joint Meeting of the United States Sections of the Combustion Institute* [CD-ROM], Combustion Inst., Pittsburgh, PA, 2001.

[10]Lutz, A. E., Kee, R. J., Grcar, J. F., and Rupley, F. M., Sandia National Labs., Rept. SAND96-8243, Livermore, CA, 1997.

[11]Sarofim, A. F., and Zhang, H. R., "Numerical Combustion of Aviation Fuel Part I: A Cross-Model Comparison of n-Heptane Premixed Flame," *2003 Fall Meeting of the Western States Section of the Combustion Institute* [CD-ROM], Combustion Inst., Pittsburgh, PA, 2003.

[12]Fairweather, M., Jones, W. P., and Lindstedt, R. P., "Predictions of Radiative Transfer from a Turbulent Reacting Jet in a Cross-Wind," *Combustion and Flame*, Vol. 89, 1992, pp. 45–63.

[13]Sivathanu, Y. R., and Gore, J. P., "Coupled Radiation and Soot Kinetics Calculations in Laminar Acetylene/Air Diffusion Flames," *Combustion and Flame*, Vol. 97, 1994, pp. 161–172.

[14]Gore, J. P., Lim, J., Takeno, T., and Zhu, X. L., "A Study of the Effects of Thermal Radiation on the Structure of Methane/Air Counter-Flow Diffusion Flames Using Detailed Chemical Kinetics," *5th ASME/JSME Joint Thermal Engineering Conference* [CD-ROM], American Society of Mechanical Engineers, Fairfield, NJ, 1999.

[15]Crosbie, A. L., and Viskanta, R., "The Exact Solution to a Simple Nongray Radiative Transfer Problem," *Journal of Quantitative Spectroscopy and Radiative Transfer*, Vol. 9, 1969, pp. 553–568.

[16]Zhu, X. L., Gore, J. P., Karpetis, A. N., and Barlow, R. S., "The Effects of Self-Absorption of Radiation on Opposed Flow Partially Premixed Flame," *Combustion and Flame*, Vol. 129, 2002, pp. 342–345.

[17]Kim, O. J., Gore, J. P., Viskanta, R., and Zhu, X. L., "Prediction of Self-Absorption in Opposed Flow Diffusion and Partially Premixed Flames Using a Weighted Sum of Gray Gases Model (WSGGM)–Based Spectral Model," *Numerical Heat Transfer, Applications*, Vol. 44, 2003, pp. 335–353.

[18]Kim, O. J., Zhu, X. L., Viskanta, R., and Gore, J. P., "Prediction of Self-absorption of Radiation from Soot Particles in Opposed Flow Diffusion Flames," *Third Asia–Pacific Conference on Combustion*, Combustion Inst., Pittsburgh, PA, 2001, pp. 368–372.

C. Kaplan
Associate Editor

Comparing the *N*-Branch Genetic Algorithm and the Multi-Objective Genetic Algorithm

Eric T. Martin,* Rania A. Hassan,† and William A. Crossley‡
Purdue University, West Lafayette, Indiana 47907-1282

Nomenclature

c	=	penalty multiplier
E	=	material Young's modulus
f	=	fitness function
g	=	inequality constraint function
h	=	equality constraint function
J	=	number of inequality constraints

Received 10 February 2003; revision received 26 February 2004; accepted for publication 5 March 2004.

*Graduate Student, School of Aeronautics and Astronautics; currently Engineer, ATA Engineering, Inc., San Diego, CA 92130; eric.martin@ata-e.com.

†Graduate Student, School of Aeronautics and Astronautics; currently Postdoctoral Associate, Engineering Systems Division, Massachusetts Institute of Technology, Cambridge, MA 02139; rhassan@mit.edu. Member AIAA.

‡Associate Professor, School of Aeronautics and Astronautics, 1282 Grissom Hall; crossley@purdue.edu. Associate Fellow AIAA.

K = number of equality constraints
N_{obj} = number of objective functions
P^* = penalty scaling factor
x = design variable vector
γ = material weight density
σ_a = material allowable stress
ϕ = objective function

Introduction

THIS Note discusses the N-branch tournament genetic algorithm (GA), a generalization of the two-branch tournament,[1,2] for multi-objective optimization and compares it to a version of the multi-objective GA (MOGA), a popular method. There are numerous MOGA implementations; all use a single rank-based fitness function to generate Pareto-optimal solutions with a traditional selection operator. The N-branch tournament GA utilizes a modified selection operator in which the population competes on separate fitness functions—a different approach to generate Pareto-optimal designs from that of MOGA and its relatives. The N-branch tournament and MOGA are evaluated in terms of the number and distribution of the solutions obtained for a set of simple, but illustrative, greater-than-two objective problems.

Multiobjective Optimization

Multi-objective optimization seeks to minimize (maximize) a vector function whose components are individual objectives. In most multi-objective problems, the solution is a family of designs called the Pareto-optimal set.[3] For each Pareto-optimal design, there is no other feasible design better on all objectives; these designs are nondominated. It is desirable to examine tradeoffs among competing objectives by finding many Pareto-optimal designs. These designs are often plotted in objective space and are referred to as the Pareto front.

Genetic Algorithm

The GA mimics survival of the fittest observed in nature and uses this concept to perform optimization-like tasks.[4] Because the GA can search discontinuous, nonconvex design spaces and because it is a population-based search, the GA has been used for multi-objective design of aerospace systems. Some examples of MOGA-based optimization for aircraft can be found in Refs. 5–7 and for space systems in Refs. 8 and 9.

Multiobjective Genetic Algorithm (MOGA)

MOGA, initially developed by Fonseca and Fleming,[10] represents the basic fitness-based approach for multiobjective optimization via a GA. Many authors have subsequently presented versions of nonaggregating, Pareto-based GA approaches that use nondominance ranking to assign fitness values for multi-objective optimization. References 11 and 12 describe and compare many of these fitness-based approaches. MOGA has been implemented by several researchers (see Refs. 13 and 14 as just two examples). Fitness-based approaches replace the multiple objectives with one fitness function and treat the problem as a typical minimization. Designs receive a rank value based on their degree of nondominance. Nondominant individuals are assigned the lowest (best) rank; highly dominated individuals, the highest (worst) rank. Each individual's fitness value is based on this rank. This scheme is often coupled with a stochastic selection operator so that noninferior individuals are more likely to survive and produce offspring for the next generation. As this repeats, the population evolves toward the Pareto-optimal set.

In this investigation, Kurapati et al.'s version of MOGA with constraint handling[15] was used. This version includes universal sampling selection and single-point crossover. Feasible, noninferior designs are stored in an approximate Pareto set that is updated after each generation as new designs dominating previously stored designs are found.

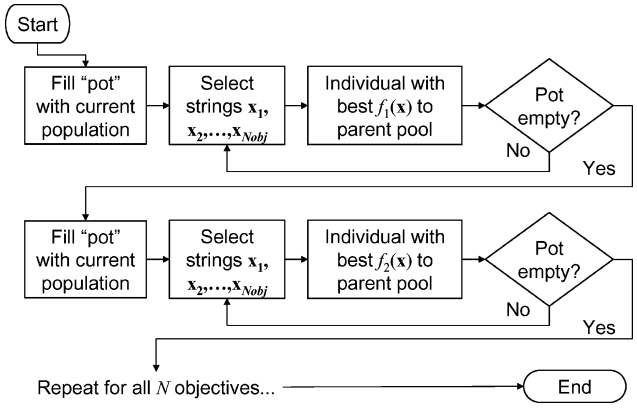

Fig. 1 N-branch tournament selection flowchart.

N-Branch Tournament Selection

The N-branch tournament GA generalizes the two-branch tournament GA.[1] The N-branch tournament differs from nondominance ranking approaches because it uses the selection operator to perform multi-objective design rather than formulating a single fitness function. In N-branch tournament selection, designs compete once on a fitness value associated with each objective. To accomplish this, the population is copied into a "pot," from which N_{obj} individuals are randomly selected without replacement to compete on the first fitness function. The best performing of the N_{obj} designs is added to the "parent pool." The first fitness competition repeats until the pot is empty. The pot is then refilled with the original population, and the tournament repeats for other objectives. After the final branch, the parent pool is full. Figure 1 illustrates this process.

To solve constrained problems, the N-branch tournament uses an exterior penalty function approach with a modification to equally penalize all objectives. The first fitness function f_1 is computed using Eq. (1):

$$f_1(\boldsymbol{x}) = \phi_1(\boldsymbol{x}) + \sum_{j=1}^{J} c_j \max[0, g_j(\boldsymbol{x})] + \sum_{k=1}^{K} c_k |h_k(\boldsymbol{x})| \quad (1)$$

Equation (2) computes a penalty-scaling factor for subsequent fitness functions:

$$P^* = 1 + |(f_1 - \phi_1)/\phi_1| \quad (2)$$

All other fitness functions are calculated with Eq. (3):

$$f_i = P^* \phi_i \qquad i = 2, \ldots, N_{\text{obj}} \quad (3)$$

The penalty-scaling factor penalizes all objectives of an infeasible design with the same percentage that penalized the first.

Once parents are selected and paired, uniform crossover generates children. After each generation, the set of feasible, noninferior designs is stored. This approximation to the Pareto set is updated as designs in a current generation dominate stored designs.

Procedure and Test Problems

To evaluate the N-branch and MOGA methods, both generated solutions for a test problem suite. Comparisons were made based on the number of solutions generated and the uniformity of the distribution of these solutions.

Test Problems

There are few discussions of benchmark problems for MOGAs. One such discussion is provided by Deb[16] who, while providing suggestions for benchmarks, also indicates that there is a lack of benchmark problem studies for MOGAs. Here, four simple problems with features representative of more complex problems were used. The first two are contrived problems. The third is a modified single-objective benchmark problem, and the fourth is a combinatorial version of a benchmark structural optimization problem.

Table 1 Material properties for the combinatorial 10-bar truss problem

Material	E, lb/in.^{2} (Pa)	γ, lb/in.^{3} (ρ, kg/m^3)	σ_a, lb/in.^{2} (Pa)	Cost, \$/lb (\$/kg)
Aluminum	10.0×10^6 (68.9×10^9)	0.101 (2800)	25.0×10^3 (172×10^6)	3.5 (7.70)
Titanium	16.5×10^6 (114×10^9)	0.162 (4480)	73.3×10^3 (505×10^6)	30.0 (66.00)
Steel	28.0×10^6 (193×10^9)	0.284 (7860)	20.0×10^3 (138×10^6)	1.0 (2.20)
Nickel	30.0×10^6 (207×10^9)	0.318 (8800)	13.3×10^3 (91.7×10^6)	20.0 (44.00)

Simple Constrained Problem

This problem demonstrates performance when constraints impact regions of a Pareto front. Three objectives are formulated as the distance to the three points in a plane as shown in Eqs. (4–6). Constraints enforce a minimum allowable distance to two additional points as described in Eqs. (7) and (8).

Minimize

$$\phi_1 = (x_1 - 4)^2 + x_2^2 \tag{4}$$

Minimize

$$\phi_2 = (x_1 + 4)^2 + x_2^2 \tag{5}$$

Minimize

$$\phi_3 = x_1^2 + (x_2 - 4)^2 \tag{6}$$

subject to

$$g_1 = 1 - \frac{\left[(x_1 + 4)^2 + (x_2 - 4)^2\right]}{3.5^2} \leq 0 \tag{7}$$

$$g_2 = 1 - \frac{\left[(x_1 + 1)^2 + (x_2 - 2.5)^2\right]}{3.5^2} \leq 0 \tag{8}$$

The two variables were identically encoded to binary strings for MOGA and N-branch GA using 13 bits per variable. The upper and lower bounds on each variable were ± 8.0. Population size and mutation rate were 108 and 0.0048, respectively, based on guidelines.[17]

Adjacent Minima Problem

This problem is similar to the first; the objectives are to minimize the distance to three points. However, this problem has two objectives that have adjacent minima. The minima of the second and third objectives are close in the design space, and so designs performing well on ϕ_2 will likely have good ϕ_3 performance. Equations (9–11) describe the objectives.

Minimize

$$\phi_1 = (x_1 - 4)^2 + x_2^2 \tag{9}$$

Minimize

$$\phi_2 = (x_1 + 4)^2 + x_2^2 \tag{10}$$

Minimize

$$\phi_3 = (x_1 + 3)^2 + (x_2 - 1)^2 \tag{11}$$

The variables were encoded as in the first problem; population size and mutation rate were also unchanged.

Modified Golinski Speed Reducer

The third problem is a variation of Golinski's speed reducer.[18,§] This problem's original single objective form has 11 inequality constraints and bounds on the 7 variables. Two active constraints of the original problem's published solution were converted to objectives, so that the multi-objective version minimizes weight of the speed reducer and stress in each of the two drive shafts as described in Eqs. 12–14.

Minimize

$$\phi_1 = 0.7854 x_1 x_2^2 \left(3.3333 x_3^2 + 14.9334 x_3 - 43.0934\right) - 1.508 x_1 \left(x_6^2 + x_7^2\right) + 7.477 \left(x_6^3 + x_7^3\right) + 0.7854 \left(x_4 x_6^2 + x_5 x_7^2\right) \tag{12}$$

Minimize

$$\phi_2 = \frac{\left[(745 x_4 / x_2 x_3)^2 + 16.9 \times 10^6\right]^{0.5}}{0.1 x_6^3} \tag{13}$$

Minimize

$$\phi_3 = \frac{\left[(745 x_5 / x_2 x_3)^2 + 157.5 \times 10^6\right]^{0.5}}{0.1 x_7^3} \tag{14}$$

The remaining nine constraints and variable bounds are unchanged from Ref. 18. For each variable, a resolution of 0.01 was desired to match the number of significant digits in the published results; this led to a chromosome length of 48 bits. Population size and mutation rate were set at 216 and 0.0027, respectively.[17]

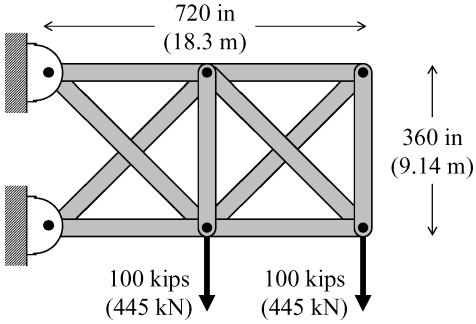

Fig. 2 Geometry and loading for the 10-bar truss problem.

Truss Problem

The fourth problem is a variation of the 10-bar truss.[1,19] Traditionally, the objective is to minimize weight, subject to stress and displacement constraints. Here the displacement is treated as a second objective and cost as a third. Variables are the cross-sectional areas of the truss elements. To investigate performance on combinatorial problems, material selection is included as a discrete variable with four possible material choices for each truss member. With this formulation, there are 1,048,576 (or 10^4) possible combinations of materials. All three objectives include the effects of material selection, and the constraints enforce yield stress limits based on the material selected for each truss element.

Each variable used 10 bits for coding. The maximum value for these was 40.0 in.^{2} (25.8×10^3 mm^2) and the minimum was 0.1 in.^{2} (64.5 mm^2). The truss geometry, loads, and boundary conditions appear in Fig. 2. The discrete variables are coded with 2 bits. Table 1 shows the material properties used; cost values are from Ref. 20. The total chromosome length was 120 bits; the population size, 480; and mutation rate, 0.00105.

§Data available on-line at http://mdob.larc.nasa.gov/mdo.test/class2prob4.html [cited 29 April 2002].

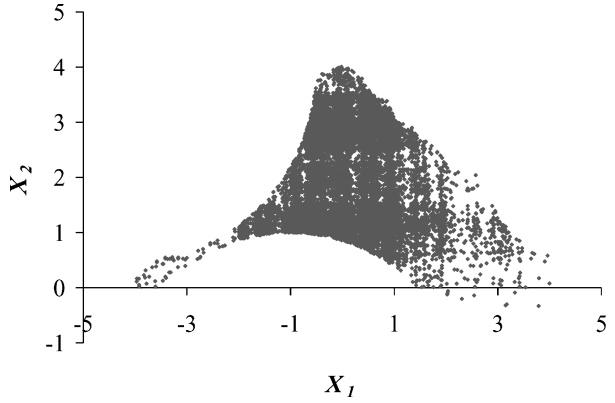

Fig. 3 Nondominated designs found by the *N*-branch GA for the simple constrained problem.

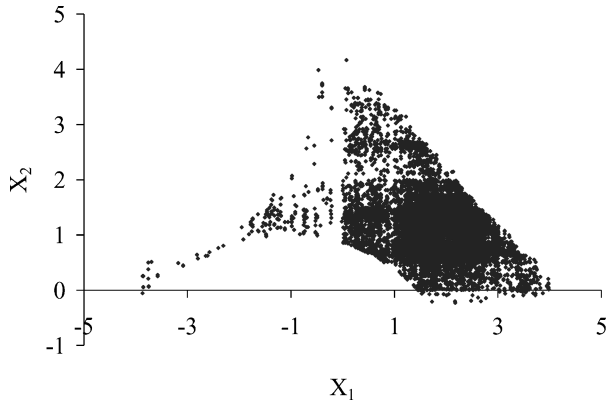

Fig. 4 Nondominated designs found by the MOGA for the simple constrained problem.

Results

The test problems were solved using MOGA and *N*-branch GA. In all investigations, the GA ran for 250 generations, and so both approaches expended the same computational effort. For each problem, both GA methods were run 10 times with different random starting seeds to assess repeatability. Graphical results shown are those of 1 run and are typical of all 10 runs.

Simple Constrained Problem

This problem is designed such that the Pareto set has a narrow "corridor" caused by two constraints described in Eqs. (7) and (8). Design space plots (x_1 vs x_2) typical of all the nondominated designs found by *N*-branch GA and MOGA appear in Figs. 3 and 4, respectively. The *N*-branch GA consistently finds more designs than MOGA near the minimum ϕ_2 endpoint ($x_1 = -4$, $x_2 = 0$) closest to the active constraint boundaries. Both approaches find designs near the unconstrained minima and resolve the unconstrained portion of the Pareto set. However, MOGA favors the Pareto set region far from the constraint boundaries. The *N*-branch GA shows no such preference. For one of the 10 random starting seeds, the MOGA approach failed to find any designs in the corridor. On average, *N*-branch tournament GA found 15,990 nondominated designs; MOGA, 11,992.

Adjacent Minima Problem

This problem demonstrates performance when minima of two objectives (here, ϕ_2 and ϕ_3) are very similar. Typical design space plots of the approximate Pareto sets for *N*-branch GA and MOGA are presented in Figs. 5 and 6, respectively. Gaps appear in the set where *N*-branch GA is unable to find many designs. MOGA, however, resolves the set with uniform density. The *N*-branch GA found more total designs than MOGA, but most are located near the ϕ_2–ϕ_3 side of the Pareto front. The *N*−branch tournament found, on average over 10 runs, 16,753 nondominated designs, whereas MOGA found 12,178.

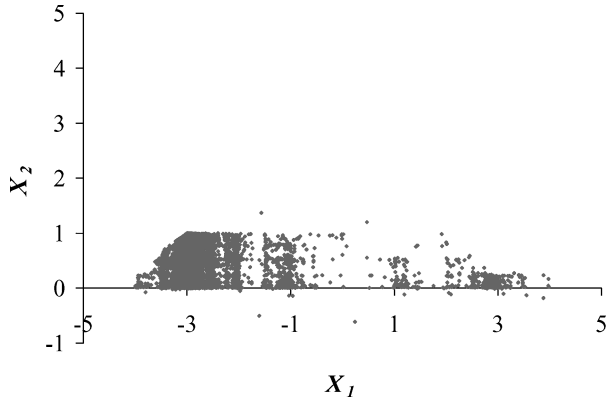

Fig. 5 Nondominated designs found by the *N*-branch GA for the similar objective problem.

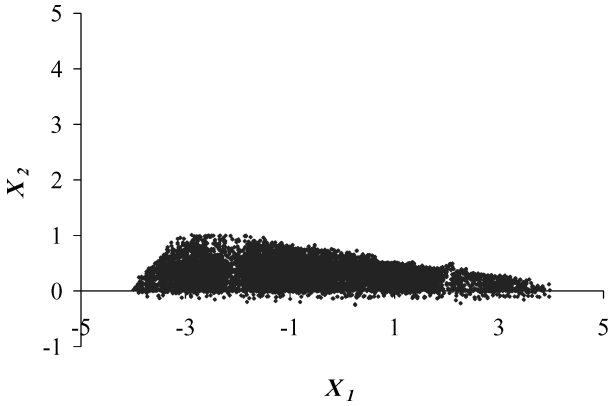

Fig. 6 Nondominated designs found by the MOGA for the similar objective problem.

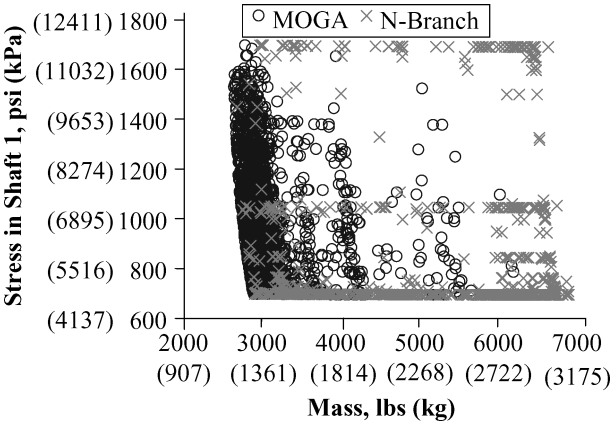

Fig. 7 Nondominated designs in weight–stress (ϕ_1–ϕ_2) space for the speed reducer problem.

Golinski's Speed Reducer

Results for this problem are presented using a Pareto front plotted in objective space. Both *N*-branch and MOGA are able to resolve a three-sided Pareto front. Figure 7 shows the nondominated designs found by both approaches for direct comparison. *N*-branch GA finds more designs minimizing the stress objectives but has gaps in the Pareto set, whereas MOGA finds more uniformly distributed minimum weight designs. This problem is highly constrained and has adjacent minima. Geometry constraints result in adjacent stress objectives; a feasible design that has low stress in one shaft likely has low stress in the other. The leading edge in this plot (low weight, low stress) looks similar to previous two-objective results,[15,21] except that lower weights are now possible due to the removal of one stress

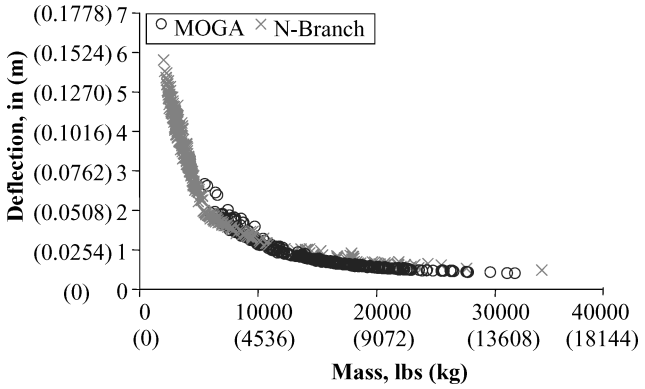

Fig. 8 Nondominated designs in weight–deflection space for the truss problem.

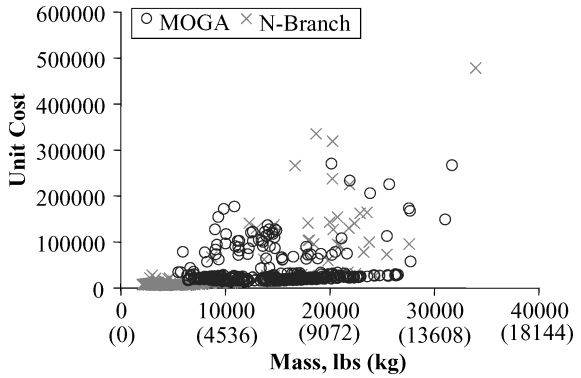

Fig. 9 Nondominated designs in weight-cost space for the truss problem.

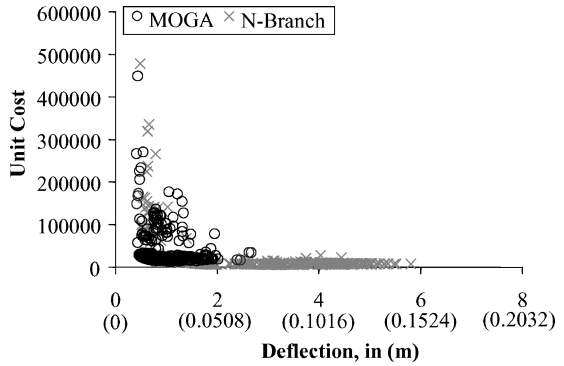

Fig. 10 Nondominated designs in cost-deflection space for the truss problem.

constraint. Overall, the MOGA finds many more nondominated designs than the N-branch GA for this problem. The N-branch tournament found, on average, 1064 nondominated designs, whereas MOGA found 2900 nondominated designs.

Truss Problem

Both the MOGA and N-branch GA generate approximate Pareto fronts for this constrained, combinatorial, three-objective problem. Figures 8–10 compare the nondominated designs found by both approaches. Figure 8 shows that the$N$-branch GA finds more designs on the low-weight side of the Pareto front, where stress constraints become active. Low-weight designs found by the N-branch GA dominate those found by the MOGA; however, low-deflection designs found by the MOGA dominate those found by the N-branch GA. This result is similar to a previous two-objective comparison.[21] Figures 9 and 10 show that, as weight and stiffness increase, the available range in cost options also increases because a greater range of materials are feasible as the stress constraints become less critical. Each approach has an even distribution of points across its Pareto front approximation. The N-branch tournament found, on average, 423 nondominated designs; and MOGA, 363.

Conclusions

An investigation using four test cases compared performance of a selection-based and a ranking fitness-based GA approach on different types of three-objective problems. For these problems, both approaches reasonably approximate the Pareto set.

Results of the simple constrained and 10-bar truss problems suggest that the N-branch GA is better suited to solving constrained problems. The adjacent minima problem results favor the MOGA approach. Golinski's speed reducer is both highly constrained and has two similar objectives, and it is not clear which approach is preferred here. The MOGA finds more evenly distributed points on the Pareto front than the N-branch GA; however, the N-branch GA finds better solutions near the extremes of the Pareto set where constraints are active.

Based on the investigations, it is difficult to make a definitive choice for the preferred MOGA approach. Like many aspects of the GA, the choice appears problem dependent. It seems that the N-branch tournament GA is preferred for three-objective problems with solutions that have numerous active constraints. The MOGA appears preferred for problems in which two or more objectives are adjacent in the design space. However, for many engineering problems, it may not be known whether two or more objectives are adjacent a priori. The success of the N-branch tournament GA demonstrates that a selection-based method can generate multi-objective solutions that are comparable to those generated by a nondominance ranking method.

Acknowledgment

This work was supported in part by NASA Collaborative Agreement NCC-1-01042 with NASA Langley Research Center.

References

[1]Crossley, W., Cook, A., Fanjoy, D., and Venkayya, V., "Using the Two-Branch Tournament Genetic Algorithm for Multiobjective Design," *AIAA Journal*, Vol. 37, No. 2, 1999, pp. 261–275.

[2]Fanjoy, D., Beaver, A., and Crossley, W., "Empirical Studies of Population Size and Parent Mixing for a Multiobjective Genetic Algorithm," AIAA Paper 2000-4892, Sept. 2000.

[3]Vincent, T., and Grantham, W., *Optimality in Parametric Systems*, 1st ed., Wiley, New York, 1981, pp. 72–103.

[4]Goldberg, D., *Genetic Algorithms in Search, Optimization, and Machine Learning*, 1st ed., Addison–Wesley, Reading, MA, 1989, pp. 19–63.

[5]Obayashi, S., Yamaguchi, Y., and Nakamura, T., "Multiobjective Genetic Algorithm for Multidisciplinary Design of Transonic Wing Planform," *Journal of Aircraft*, Vol. 34, No. 5, 1997, pp. 690–692.

[6]D'Souza, B., and Simpson, T., "A Genetic Algorithm Based Method for Product Family Design Optimization," *Engineering Optimization*, Vol. 35, No. 1, 2003, pp. 1–18.

[7]Crossley, W. A., Martin, E. T., and Fanjoy, D. W., "A Multiobjective Investigation of 50-Seat Commuter Aircraft Using a Genetic Algorithm," AIAA Paper 2001-5247, Oct. 2001.

[8]Hassan, R., and Crossley, W., "Multi-Objective Optimization of Communication Satellites with Two-Branch Tournament Genetic Algorithm," *Journal of Spacecraft and Rockets*, Vol. 40, No. 2, 2003, pp. 266–272.

[9]Hartmann, J., Coverstone-Carroll, V., and Williams, S., "Optimal Interplanetary Spacecraft Trajectories via a Pareto Genetic Algorithm," *Journal of Astronautical Sciences*, Vol. 46, No. 3, 1998, pp. 267–282.

[10]Fonseca, C., and Fleming, P., "Genetic Algorithms for Multiobjective Optimization: Formulation, Discussion and Generalization," *Proceedings of the Fifth International Conference on Genetic Algorithms*, edited by S. Forrest, Morgan Kaufmann, San Mateo, CA, 1993, pp. 416–423.

[11]Coello Coello, C., "An Updated Survey of GA-Based Multiobjective Optimization Techniques," *ACM Computing Surveys*, Vol. 32, No. 2, 2000, pp. 109–143.

[12]Zitzler, E., Deb, K., and Thiele, L., "Comparison of Multiobjective Evolutionary Algorithms: Empirical Results," *Evolutionary Computation*, Vol. 8, No. 2, 2000, pp. 173–195.

[13]Obayashi, S., Tsukahara, T., and Nakamura, T., "Multiobjective Genetic Algorithm Applied to Aerodynamic Design of Cascade Airfoils," *IEEE Transactions on Industrial Elecronics*, Vol. 47, No. 1, 2000, pp. 211–216.

[14]Cheng, F., and Li, D., "Multiobjective Optimization Design with Pareto Genetic Algorithm," *Journal of Structural Engineering*, Vol. 123, No. 9, 1997, pp. 1252–1261.

[15]Kurapati, A., Azarm, S., and Wu, J., "Constraint Handling in Multiobjective Genetic Algorithms," AIAA Paper 2000-4893, Sept. 2000.

[16]Deb, K., "Multi-Objective Genetic Algorithms: Problem Difficulties and Construction of Test Problems," *Evolutionary Computation*, Vol. 7, No. 3, 1999, pp. 205–230.

[17]Williams, E., and Crossley, W., "Empirically-Derived Population Size and Mutation Rate Guidelines for a Genetic Algorithm with Uniform Crossover," *Soft Computing in Engineering Design and Manufacturing*, edited by P. Chawdhry, R. Roy, and R. Pant, Springer-Verlag, London, 1998, pp. 163–172.

[18]Townsend, J., "Golinski's Speed Reducer," *MDOB Test Suite*, NASA Langley Research Center, Hampton, VA, 2002.

[19]Venkayya, V., and Tischler, V., "Design of Optimum Structures," *Computers and Structures*, Vol. 1, Nos. 1/2, 1971, pp. 265–309.

[20]Farag, M., "Economics of Materials and Processes," *Materials Selection for Engineering Design*, 1st ed., Prentice–Hall, London, 1997, pp. 209–226.

[21]Martin, E., and Crossley, W., "Empirical Studies of Selection Method for Multiobjective Genetic Algorithm," AIAA Paper 2002-0177, Jan. 2002.

A. Messac
Associate Editor

Errata

Geometrically Exact, Intrinsic Theory for Dynamics of Curved and Twisted Anisotropic Beams

Dewey H. Hodges
Georgia Institute of Technology, Atlanta, Georgia 30332-0150

[AIAA Journal, 41(6), pp. 1131–1137 (2003)]

THE sentence that starts on the second line after Eq. (34) should read, "A clamped boundary at the other end yields a two-point boundary-value problem for which $C(\ell) = \Delta$." Here Δ is the 3×3 identity matrix.